

Supporting information for
Ultrafast electron dynamics in coupled and uncoupled HgTe quantum dots

S.G. Mizrahi[†],¹ M. Weis[†],¹ E. Péronne,¹ A. Kies,¹ A. Khalili,² Y. Prado,² S. Sauvage,³ E. Lhuillier,² and D. Boschetto*¹

¹*Laboratoire d'Optique Appliquée, ENSTA Paris, CNRS, Ecole Polytechnique,
Institut Polytechnique de Paris, 91761 Palaiseau, France*

²*Sorbonne Université, CNRS, Institut des NanoSciences de Paris, 4 place jussieu, 75005 Paris, France*

³*C2N, Centre de Nanosciences et de Nanotechnologies,
Université Paris-Saclay, CNRS, 91120 Palaiseau, France*

(Dated: December 5, 2024)

I. SAMPLES PREPARATION

Chemicals: Mercury chloride (HgCl₂, Sigma-Aldrich, 99%), tellurium powder (Te, Sigma-Aldrich, 99.99%), trioctylphosphine (TOP, Alfa, 90%), oleylamine (OLA, Acros, 80-90%), dodecanethiol (DDT, Sigma-Aldrich, 98%), 2-mercaptoethanol (MPOH, Merck, >99%), and N,N dimethylformamide (DMF, VWR), toluene (VWR, 99.8%) were used. All chemicals were used without further purification, except oleylamine that is centrifuged before use. **Mercury compounds are highly toxic. Handle them with special care.**

1 M TOP:Te precursor: 2.54 g of Te powder was mixed with 20 mL of TOP in a three-neck flask. The flask was kept under vacuum at room temperature for 5 min before the temperature was raised to 100°C. Degassing was conducted at this temperature for 20 min. Next, the atmosphere was switched to N₂ and the temperature was raised to 275°C. The solution was stirred until a clear orange coloration was obtained. The flask was then cooled down to room temperature and the color turned to yellow. Finally, this solution was transferred to a nitrogen-filled glove box for storage.

HgTe nanocrystals emitting at 2 μm: In a 100 mL three neck flask, 543 mg of HgCl₂ and 50 mL of oleylamine were degassed under vacuum at 110°C for 1 h. Meanwhile, 2 mL of TOP:Te (1 M) were extracted from the glove box and mixed with 8 mL of oleylamine. After that the atmosphere was switched to N₂ and the temperature was set as 70°C. When the temperature stabilized, the TOP:Te solution was quickly injected. After 3 min of reaction, 10 mL of DDT/Toluene (1:9 in volume) solution was injected and a water bath was used to quench the reaction. The nanocrystals were precipitated with methanol and redispersed in CHCl₃ twice. After that, the nanocrystals dispersed in CHCl₃ were centrifugated to remove the unstable phase. The stable phase was precipitated again with methanol and stored in toluene.

HgTe ink preparation: 10 mg of HgCl₂, 2 mL of MPOH, and 18 mL of DMF are mixed to form an exchange solution. 0.25 mL of this exchange solution and 0.5 mL of DMF are added to 0.25 mL of HgTe NCs in toluene. Phase dissociation occurs when a few drops of hexane are added to the mixture: the dark bottom phase is where the NCs migrate while the top transparent phase can be removed with a plastic pipette. This washing step is repeated twice before adding a few mL of toluene. The mixture is then centrifuged at 6000 rpm for 4 minutes. The supernatant is discarded while the formed solid pellets of NCs can be re-dispersed in 100 μL of DMF to obtain the ink of HgTe. A few cycles of sonication - vortex - centrifugation can help promote particle dispersion.

Film deposition: A single side polished sapphire wafer is cleaned by sonication in an acetone batch. The substrate is then further cleaned by a flow of acetone and isopropanol before being dried. For uncoupled film we spin coated the solution of nanocrystal in toluene. For uncoupled uncoupled nanocrystals, the pristine solution is directly spin coated on the same substrate. For coupled nanocrystals we use the HgTe ink solution. A few drops of DMF are spread on the surface of the patterned sapphire substrate before a spin-coating at 3000 rpm for 30s. This step is necessary to promote the adhesion between the sapphire surface and the NC ink. Then we deposit one drop of the ink solution on the substrate and conduct a two steps spin-coating. First, speed is set at 1500 rpm for 240 s and then the film is dried using a higher speed (2500 rpm) for 60 s. A smooth film of HgTe NCs is formed.

[†] These authors contributed equally to this work.

* Corresponding author: Davide.Boschetto@ensta.fr

II. ELECTRONIC STRUCTURE CALCULATIONS

In order to explain the experimental results, we conducted numerical simulations of HgTe quantum dots to get their energy spectrum and eigenstates so we could calculate the oscillator strength of the different transitions. It helps to figure out which optical transitions are possible. Unless specified otherwise, m stands for the mass of the electron in all the equations.

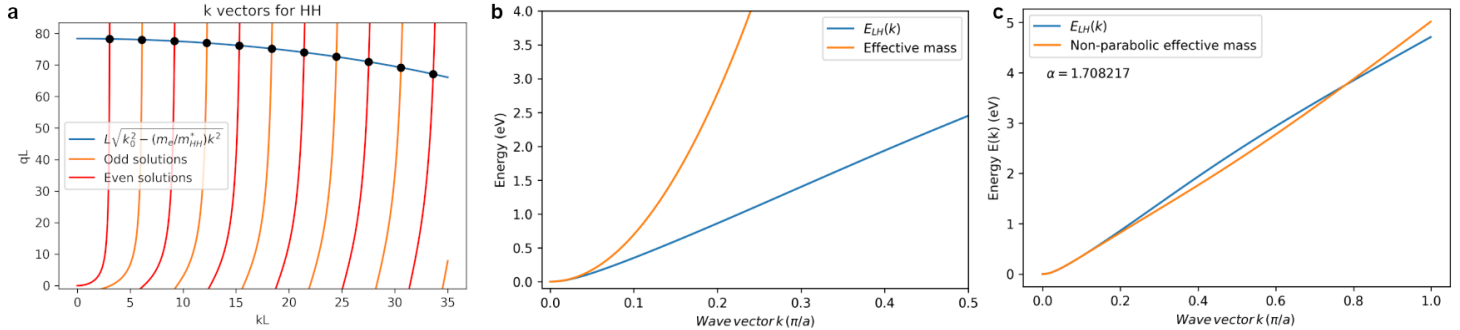


FIG. S1: (a) Geometric resolution for the HH band of HgTe. (b) Comparison of the LH band calculated with the kp 14 bands model (blue) and the parabolic band with an effective mass $m_{LH}^* = 0.013m_e$. (c) Comparison with the non-parabolic effective mass approximation.

A. HgTe Quantum dots energy spectrum

As nanocrystals are composed of a finite number of primitive cells compared to bulk crystals, ab initio approaches cannot be advantageously carried in the Fourier space as the domain needed to be considered becomes gigantic and is no longer limited to the first Brillouin zone. A more simple approach, which still provides good first order approximation of the oscillator strengths, is to apply the quantum well model to the bulk bands of the material. By treating the 3 dimensions independently, the energy levels of HgTe quantum dots sample can be retrieved for the energy levels close to the Fermi level by taking into account LH and HH bands as calculated within the k.p 14 bands model of bulk HgTe [1].

1. Resolution of the one-dimensional Schrodinger equation

In the simplest QD model, we can consider a cubic quantum dots of side length L and assumed that both bands are isotropic such that the hamiltonian of the system can be separated into three hamiltonians for each direction of space. Therefore, the eigenstates of the hamiltonian are straightforward to calculate [2][3]. For a finite potential height V_0 , the geometric solution of the confined states obeys the following conditions:

$$k_0^2 = \frac{m_{out}^*}{m_{in}^*} k_n^2 + q_n^2 \text{ with } k_0^2 = \frac{2m_{out}^*V_0}{\hbar^2} \quad (S1)$$

$$\begin{aligned} q_n &= k_n \tan(k_n L/2) \quad \text{for even solutions} \\ q_n &= -k_n \cot(k_n L/2) \quad \text{for odd solutions} \end{aligned} \quad (S2)$$

From which we deduce the eigenvalues :

$$E_n = \frac{\hbar^2 k_n^2}{2m_{in}^*} \quad (S3)$$

By using equation (S1) and the set of equations (S2), it is possible to find geometrically the solutions of the one-dimensional Schrodinger equation as shown in FigS1.a. Where $m_{out}^* = m_e$ is the electron mass, $m_{in}^* = 0.69m_e$ is the effective mass of the HH band holes in HgTe [1], L is the length of the well and the potential barrier $V_0 = 4.52$ eV. The length parameters used for our model are $L_x = 5.58$ nm, $L_y = 6.25$ nm and $L_z = 15.23$ nm.

2. Band non-parabolicity

The first conduction band of HgTe, the LH band has been shown to be highly non-parabolic [1][4] and the effective mass found for the centre of the Brillouin zone is $m_{LH}^* = 0.013m_e$ [1]. As such, the parabolic approximation is not good enough to predict the energies of the first excited states (see FigS1.b).

In order to tackle this problem, the previous equations are solved by taking into account the effective mass which depends on the energy [2] such as:

$$m^*(E(k)) = m^*(E(0))(1 + \alpha E(k))^{1/3}(1 + 2\alpha E(k))^{2/3} \quad (S4)$$

The fitting parameter α , which equals ≈ 1.7 , is adjusted in order to match the 14 bands kp model as shown in FigS1.c. Accordingly, the geometric resolution of the Schrödinger equation using the equations (S1) and (S2) combined with the fitting of the a parameter for the HH band gives the energies of the confined hole states.

3. Three dimensional system

Following the previous calculations and by treating each spatial variable independently, the eigenvalues of the Schrödinger equation for the quantum dot are computed. All the possible combinations for a set of wave vectors are calculated for the one-dimensional system of each band. For an eigenvector $|k_{n_x}, k_{n_y}, k_{n_z}\rangle$, we get:

$$E_{n_x, n_y, n_z} = \frac{\hbar^2}{2m_{in}^*} (k_{n_x}^2 + k_{n_y}^2 + k_{n_z}^2) \quad (S5)$$

From here, we will use the notation $|k\rangle$ with $k^2 = k_{n_x}^2 + k_{n_y}^2 + k_{n_z}^2$.

B. Oscillator Strength

The oscillator strength is a dimensionless quantity that express the weight of an optical transition.

1. Difference between interband and intraband transitions

In the simple model we are using, the orthogonal eigenfunctions we get are actually envelope functions defined over a single band. So, while we can easily use the equation intraband transitions :

$$f_{intra} = \frac{2}{3m(E_{k'} - E_k)} \sum_{x_i=x,y,z} |\langle k' | \hat{p}_{x_i} | k \rangle|^2 \quad (S6)$$

This equation is wrong for interband transitions because those wavefunctions do not take into account the periodicity of the crystal as Bloch functions would. For an interband transition with Bloch functions of the form $\psi_{\nu, \vec{k}}(\vec{r}) = \varphi_{\vec{k}}(\vec{r}) u_{\nu, \vec{k}}(\vec{r})$, the extradiagonal terms of the momentum operator, for a transition from a band ν to a band c , are of the form :

$$\langle \psi_{c, \vec{k}'} | \hat{\vec{p}} | \psi_{\nu, \vec{k}} \rangle = \int \varphi_{\vec{k}'}^*(\vec{r}) u_{c, \vec{k}'}^*(\vec{r}) \vec{\nabla} (\varphi_{\vec{k}}(\vec{r}) u_{\nu, \vec{k}}(\vec{r})) d^3\vec{r}$$

As the functions $u_{\nu, \vec{k}}(\vec{r})$ are orthogonal and variate much faster than the functions $\varphi_{\vec{k}}(\vec{r})$, we can write :

$$\langle \psi_{c, \vec{k}'} | \hat{\vec{p}} | \psi_{\nu, \vec{k}} \rangle = \langle \varphi_{\vec{k}'} | \varphi_{\vec{k}} \rangle \int u_{c, \vec{k}'}^*(\vec{r}) \vec{\nabla} (u_{\nu, \vec{k}}(\vec{r})) d^3\vec{r} = \langle \varphi_{\vec{k}'} | \varphi_{\vec{k}} \rangle \vec{p}_{c\nu} \quad (S7)$$

From equation (S7), the oscillator strength becomes[5] :

$$f_{inter} = \frac{2|p_{c\nu}|^2}{m(E_{k'} - E_k)} |\langle k' | k \rangle|^2 \quad (S8)$$

With this model, we were not able to access the Kane momentum $p_{c\nu}$ so we supposed it was a constant which did not depend on the \vec{k} vector and extracted the value from another publication giving the oscillator strength of the first exciton depending on quantum dot size[6]. We note that it corresponds roughly to the matrix element $P = \sqrt{E_p \hbar^2 / (2m_0)}$ with $E_p = 30$ eV as deduced from the 14-band k.p model of reference [1].

C. Density of states and joint density of states

The density of state was computed by using the textbook case of the density of states (DOS) for quantum dots [2] for which Dirac deltas have been replaced by gaussians to take into account the size distribution of the dots. This gives us the following DOS ρ_{QD} for a quantum dot with $2N$ states of energy E_n :

$$\rho_{QD}(E) = \sum_{n=0}^{N-1} \sqrt{\frac{2}{\pi\sigma_n^2}} e^{-\frac{1}{2}\left(\frac{E-E_n}{\sigma_n}\right)^2} \quad (\text{S9})$$

From there, it was possible to compute the joint density of states (JDOS) ρ_{cv} using the procedure described in reference [7]. The JDOS can be obtained using the following equation:

$$\rho_{cv}(\omega) = \frac{\beta}{2\Omega} (\rho_{QD}^c * \rho_{QD}^v)(\hbar\omega) \delta_{\vec{k}_v, \vec{k}_c} \quad (\text{S10})$$

β , Ω , ρ_{QD}^c , ρ_{QD}^v and $\delta_{\vec{k}_v, \vec{k}_c}$ are respectively a normalization constant, the volume of the quantum dot, the conduction DOS, the valence DOS and the kronecker symbol to only allow vertical transitions.

III. RELATIVE CHANGE IN REFLECTIVITY AT A RESONANT TRANSITION

We calculate the change in the real part of the refractive index Δn as a function of the changes in absorption Δk (imaginary part of the refractive index) using the Kramers-Kronig relations, under the simplified approximation that the probe frequency ω matches the energy gap ω_0 (i.e., $\omega = \omega_0$). This will allow us to understand which term dominates in driving the changes in reflectivity.

A. The simplified model

The Kramers-Kronig relations link the real and imaginary parts of a material's complex refractive index $\tilde{n}(\omega) = n(\omega) + ik(\omega)$. Specifically, the change in the real part of the refractive index $\Delta n(\omega)$ due to a change in absorption $\Delta k(\omega')$ is given by:

$$\Delta n(\omega) = \frac{1}{\pi} \mathcal{P} \int_{-\infty}^{\infty} \frac{\Delta k(\omega')}{\omega' - \omega} d\omega' \quad (\text{S11})$$

where \mathcal{P} denotes the Cauchy principal value of the integral.

Here, we make the following simplifying assumptions:

- **Probe photon frequency matches the energy gap:** $\omega = \omega_0$.
- **Significant Δk near ω_0 :** The change in absorption $\Delta k(\omega')$ is significant only near ω_0

To model $\Delta k(\omega')$, we use a Lorentzian function centered at ω_0 :

$$\Delta k(\omega') = \Delta k_0 \frac{\gamma^2}{(\omega' - \omega_0)^2 + \gamma^2} \quad (\text{S12})$$

where:

- Δk_0 is the peak of the change in absorption.
- γ is the linewidth (damping constant) of the absorption feature.

Substituting the Lorentzian form of $\Delta k(\omega')$ into the Kramers-Kronig relation:

$$\Delta n(\omega) = \frac{1}{\pi} \mathcal{P} \int_{-\infty}^{\infty} \frac{\Delta k_0 \gamma^2}{(\omega' - \omega_0)^2 + \gamma^2} \cdot \frac{1}{\omega' - \omega} d\omega' \quad (\text{S13})$$

$$= \Delta k_0 \cdot \left[\frac{\omega - \omega_0}{(\omega - \omega_0)^2 + \gamma^2} \right] \quad (\text{S14})$$

This result uses the standard Hilbert transform of a Lorentzian function.

Setting $\omega = \omega_0$:

$$\Delta n(\omega_0) = \Delta k_0 \cdot \left[\frac{\omega_0 - \omega_0}{(\omega_0 - \omega_0)^2 + \gamma^2} \right] = 0 \quad (\text{S15})$$

Therefore, at the resonance frequency, the change in the real part of the refractive index is zero.

On the other side, the changes in reflectivity ΔR can be expressed as:

$$\Delta R_{\omega_0} = \left(\frac{\partial R}{\partial n} \right)_{\omega_0} \Delta n(\omega_0) + \left(\frac{\partial R}{\partial k} \right)_{\omega_0} \Delta k(\omega_0) \quad (\text{S16})$$

But since $\Delta n(\omega_0) = 0$:

$$\Delta R_{\omega_0} \approx \left(\frac{\partial R}{\partial k} \right)_{\omega_0} \Delta k(\omega_0) \quad (\text{S17})$$

This implies that the reflectivity change ΔR at ω_0 is dominated by $\Delta k(\omega_0)$.

This calculation confirms that, at the band edge, the change in reflectivity is predominantly due to changes in absorption, and the dispersive contribution to the refractive index can be neglected in a first order approximation.

B. Estimation of the numerical values

We estimate $\left(\frac{\partial R}{\partial k} \right)_{\omega_0}$ using $n = 2.3$ and $k = 0.1$ from reference [8].

The reflectivity R at normal incidence is:

$$R = \left| \frac{n - 1 + ik}{n + 1 + ik} \right|^2 = \frac{(n - 1)^2 + k^2}{(n + 1)^2 + k^2} \quad (\text{S18})$$

whose partial derivative with respect to k is:

$$\frac{\partial R}{\partial k} = \frac{2k [(n + 1)^2 - (n - 1)^2]}{[(n + 1)^2 + k^2]^2} = \frac{8nk}{[(n + 1)^2 + k^2]^2} \quad (\text{S19})$$

Using $n = 2.3$ and $k = 0.1$:

$$\frac{\partial R}{\partial k} = \frac{8 \times 2.3 \times 0.1}{[(2.3 + 1)^2 + (0.1)^2]^2} \approx 0.01548 \quad (\text{S20})$$

Therefore:

$$\left(\frac{\partial R}{\partial k} \right)_{\omega_0} \approx 0.01548 \quad (\text{S21})$$

Moreover, we can also calculate the reflectivity R at ω_0 :

$$R = \frac{(n - 1)^2 + k^2}{(n + 1)^2 + k^2} \approx 0.15596 \quad (\text{S22})$$

C. Estimation of the changes in absorption

In a pump-probe experiment involving HgTe quantum dots, the measured relative change in reflectivity is:

$$\frac{\Delta R}{R} = 10^{-3} \quad (\text{S23})$$

From the previous calculations, we have:

$$\Delta R \approx \alpha \Delta k \quad (\text{S24})$$

where α is given by:

$$\alpha = \left(\frac{\partial R}{\partial k} \right)_{\omega_0} \approx 0.01548 \quad (\text{S25})$$

from which we can calculate the absolute change in reflectivity ΔR :

$$\Delta R = R \times \frac{\Delta R}{R} = 1.56 \times 10^{-4} \quad (\text{S26})$$

Using the relationship $\Delta R \approx \alpha \Delta k$, we can solve for Δk :

$$\Delta k = \frac{\Delta R}{\alpha} = \frac{1.56 \times 10^{-4}}{0.01548} \approx 0.01007 \quad (\text{S27})$$

The relative change in k is:

$$\frac{\Delta k}{k} = \frac{0.01007}{0.1} = 0.1007 \quad (\text{S28})$$

which means a significant relative changes of around 10% at $\omega = \omega_0$.

IV. COMPUTATION OF THE AVERAGE NUMBER OF ABSORBED PHOTONS PER QD

In order to calculate the average number of absorbed photons per QD, we need to know the absorption cross section $\sigma(\omega)$ of the film for the pump frequency ω , which is written as :

$$\sigma(\omega) = \frac{2\omega\kappa(\omega)}{cn_{QD}} \quad (\text{S29})$$

κ , c and n_{QD} are the imaginary part of the optical index, the speed of light and the density of quantum dots respectively. The value of the absorption cross section at the absorption edge of HgTe QDs has been documented in the literature and is about $\sigma(\omega_0) \approx 1 \cdot 10^{-15}$ [9]. As c and n_{QD} doesn't depend on the pump frequency, we can determine The imaginary part of the optical index is about 0.1 at the band edge while it is about 0.15 at $\omega_1 = 1.55$ eV (800 nm) [8]. By cross multiplication, we obtain :

$$\sigma(\omega_1) = \frac{\omega_1\kappa(\omega_1)}{\omega_0\kappa(\omega_0)}\sigma(\omega_0) \quad (\text{S30})$$

We finally obtain $\sigma(\omega_1) \sim 3.6 \cdot 10^{-15}$ cm². As an example, for a fluence F of 60 $\mu\text{J}/\text{cm}^2$ we get the average number of excitations per QD $\langle N \rangle = \sigma F / \hbar\omega \approx 0.86$ [10]. Previous studies have assumed the generation of excitons per QD followed a Poisson distribution [10, 11]. As such, we calculate it for different number of photons absorbed per QD N :

$$P_N = \frac{\langle N \rangle^N}{N!} e^{-\langle N \rangle} \quad (\text{S31})$$

The Poisson statistics for 0.86 excitations per QD gives about 36% of monoexcited QD and 14% of doubly excited QD. S2 shows the Poisson statistics of the different fluences we used in our experiments.

V. TRANSIENT REFLECTIVITY

Figure S3 compares the transient experimental reflectivity variation between the uncoupled (short dash line) and the coupled (full line) samples. The scale is the same for both considered low and high energy 2.2 and 1.2 wavelengths and for both samples. The relaxation at short times below 5 ps is clearly faster for the coupled QDs than for the uncoupled QDs. The measurements also show that the high energy reflectivity variation amplitude at 1.2 μm wavelength is much smaller than the low energy one at 2.2 μm wavelength (note the broken vertical scale), as a result likely of a transient strong photo-induced absorption compensating the interband absorption bleaching. We attribute this photo-induced absorption to an intraband absorption between the P-like conduction states to the D-like one, expected to exhibit a strong intraband dipole.

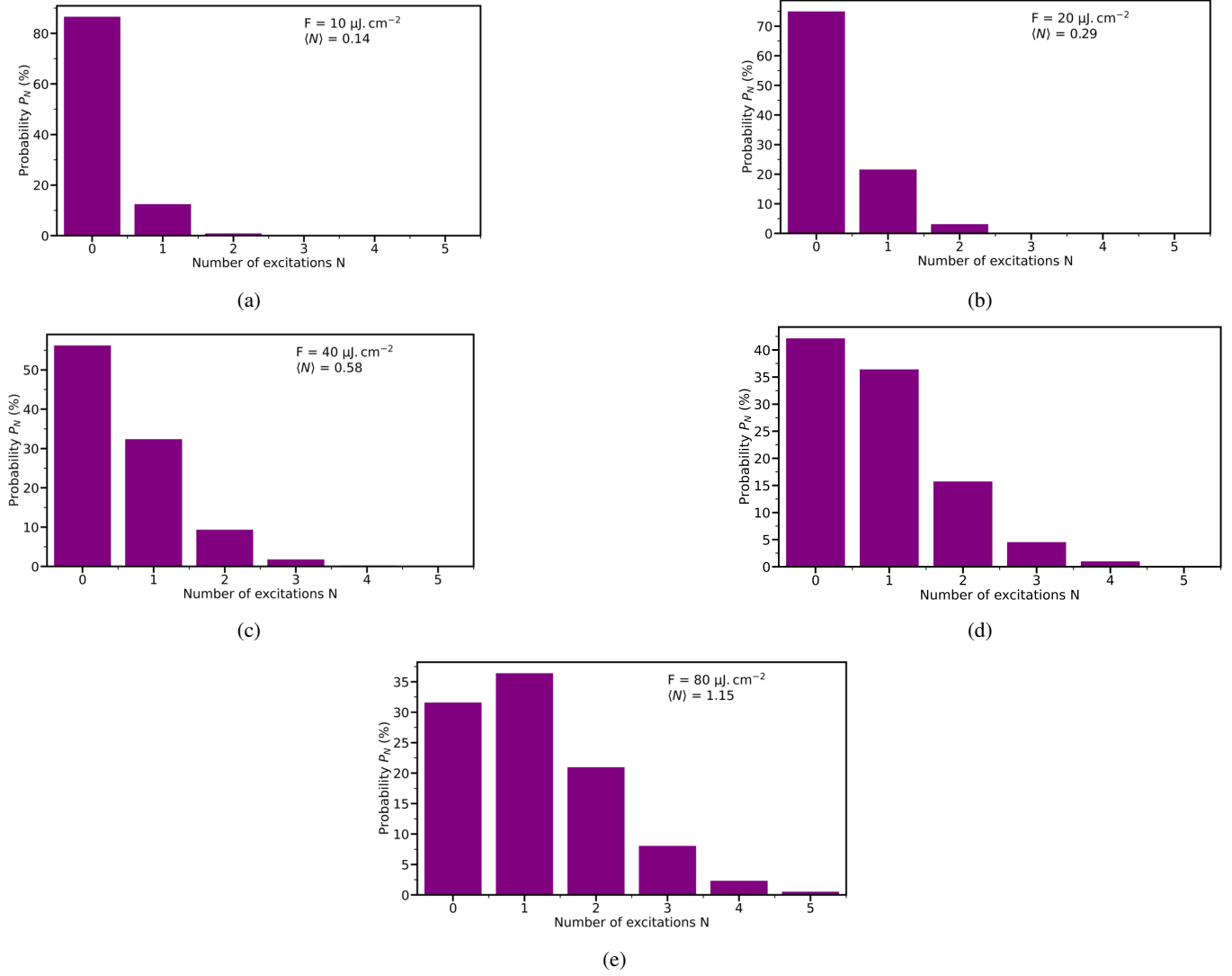


FIG. S2: Poisson distribution of excitations for several fluences between 10 and $80 \mu\text{J}/\text{cm}^2$. (a) $10 \mu\text{J}/\text{cm}^2$. (b) $20 \mu\text{J}/\text{cm}^2$. (c) $40 \mu\text{J}/\text{cm}^2$. (d) $60 \mu\text{J}/\text{cm}^2$. (e) $80 \mu\text{J}/\text{cm}^2$.

VI. MODELLING OF THE ELECTRON AND HOLE DYNAMICS

The rate equation model is written on the populations of electrons and holes averaged over the nanocrystal ensemble. The model considers 3 different mechanisms:

- intraband relaxation,
- interband Sh-Se recombination,
- multiparticle Auger recombination.

Intraband relaxation from level i to level j ($1 \leq i, j \leq 3$) is written with the two following contributions to the population rates on the initial i and final j states:

$$\frac{dN_i}{dt} = -\frac{N_i(t)}{\tau_{ij}} \quad \text{and} \quad \frac{dN_j}{dt} = +\frac{N_i(t)}{\tau_{ij}}$$

where τ_{ij} is the relaxation time from level i to level j . To account for the Pauli exclusion principle for the pseudo-levels N_{e1}

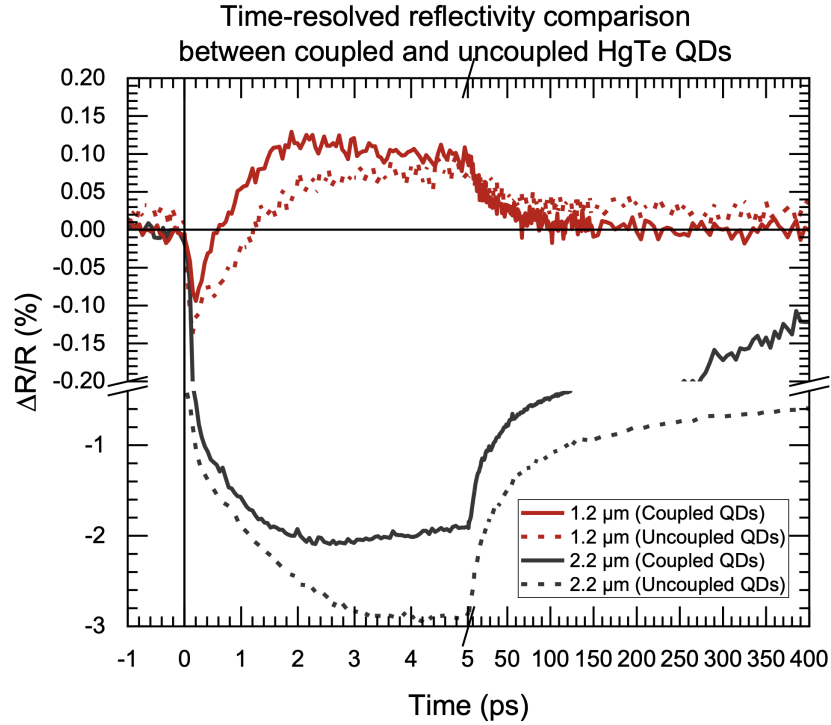


FIG. S3: Comparison between the experimental transient reflectivity variation in the sample of uncoupled (dashed line) and coupled (full line) quantum dots.

and N_{h1} with a degeneracy of only 2, the model includes the occupation factor of the relaxation towards these two levels:

$$\frac{dN_j}{dt} = + \frac{(1 - N_j/2)N_i(t)}{\tau_{ij}}.$$

To account for the interband recombination, the model only considers the recombination from the N_{e1} and N_{h1} pseudo-levels, since the other levels undergo much faster relaxation. The following form

$$\frac{dN_{e1,h1}}{dt} = - \frac{\sqrt{N_{e1}(t)N_{h1}(t)}}{\tau_{exc}}$$

corresponds to a monoexponential decay of the electron and hole ground state population with recombination time τ_{exc} and preserves the equality of the total number of electrons to the total number of holes, as shown in Figure S5.

At last, the model includes an Auger three-particle collision mechanism as described in Figure 5 (b) in the main text, with a trimolecular coefficient $1/\tau_{Auger}$ ensuring the recombination of an electron-hole pair occupying the ground level and the promotion of the second electron towards the N_{e2} pseudo-level.

Figure S4 compares the experimental reflectivity and the calculated transient differential absorption in a non-normalized linear scale (on the left) and in log scale (on the right) considering the absolute values of the quantities in this later case. The biexponential exciton recombination is clearly apparent in the transient absorption of the model and roughly in the experimental data supporting the presence of a three-particle Auger recombination mechanism.

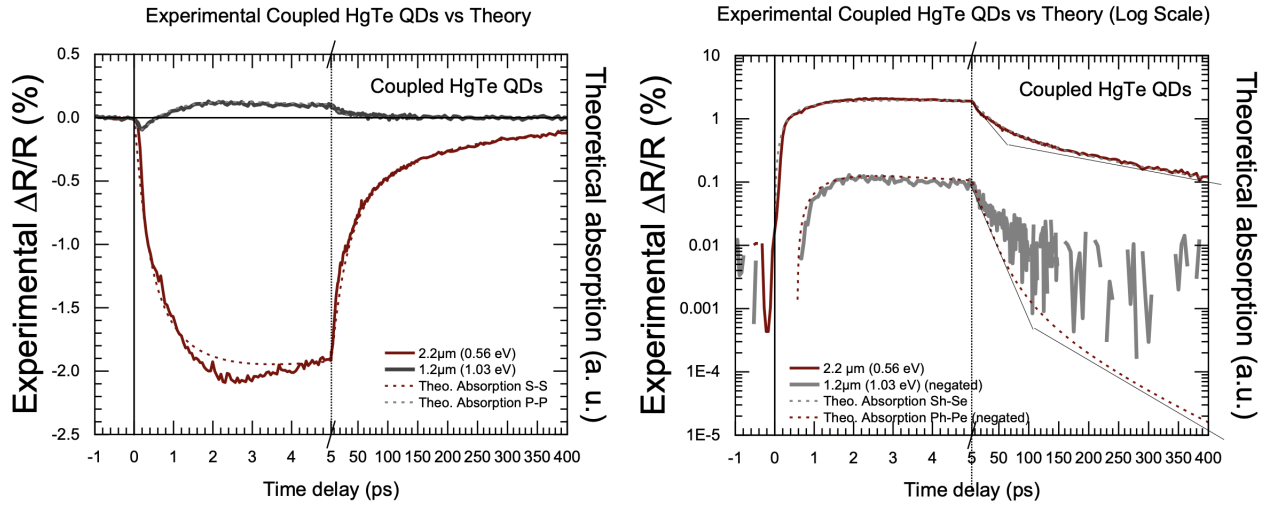


FIG. S4: Transient reflectivity change in a log scale for the coupled sample at 1.2 μm wavelength (black full line) and at 2.2 μm wavelength (red full line) and corresponding transient absorption as calculated by the dynamics rate equation model (dashed line), represented in vertical linear scale (left) and log scale (right). In the log scale, the absolute value of the reflectivity change is considered. The scales are the same and comparable experimentally for both wavelengths (no normalization) and theoretically for the $S_h - S_e$ and $P_h - P_e$ calculated absorption (same scale). The thin lines in log scale are guides to the eyes for the bi-exponential exciton recombination in the dynamics model.

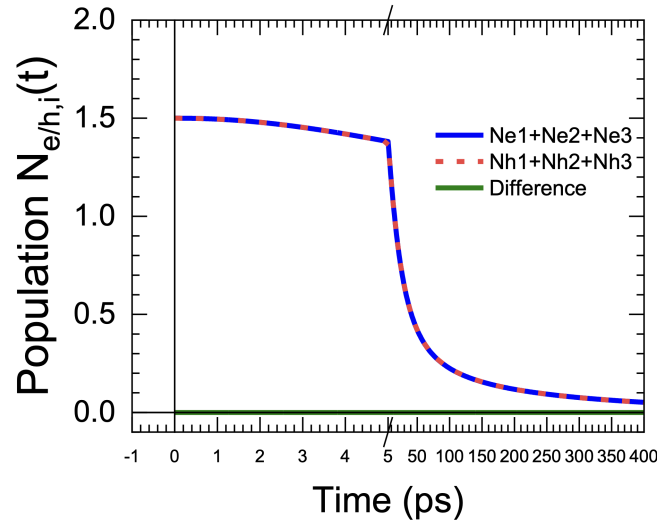


FIG. S5: Total number of electrons (full line) and holes (dashed line) as a function of time as calculated by the rate equation model. The difference (green full line) is zero at all times.

VII. EXPERIMENTAL REFLECTIVITY MEASUREMENTS WITHOUT NORMALIZATION

Figure S6 and S7 show the transient reflectivity for both uncoupled and coupled HgTe QDs, respectively, without normalization, at a pump fluence of $60 \mu\text{J}/\text{cm}^2$.

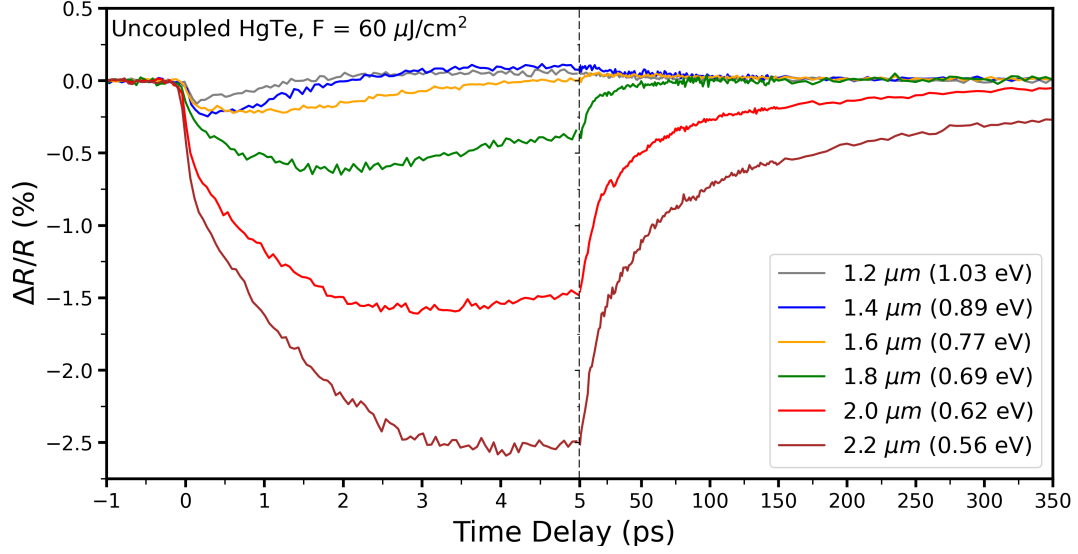


FIG. S6: Transient reflectivity versus pump-probe time delay without normalization for uncoupled HgTe QDs, at a pump fluence of $60 \mu\text{J}/\text{cm}^2$.

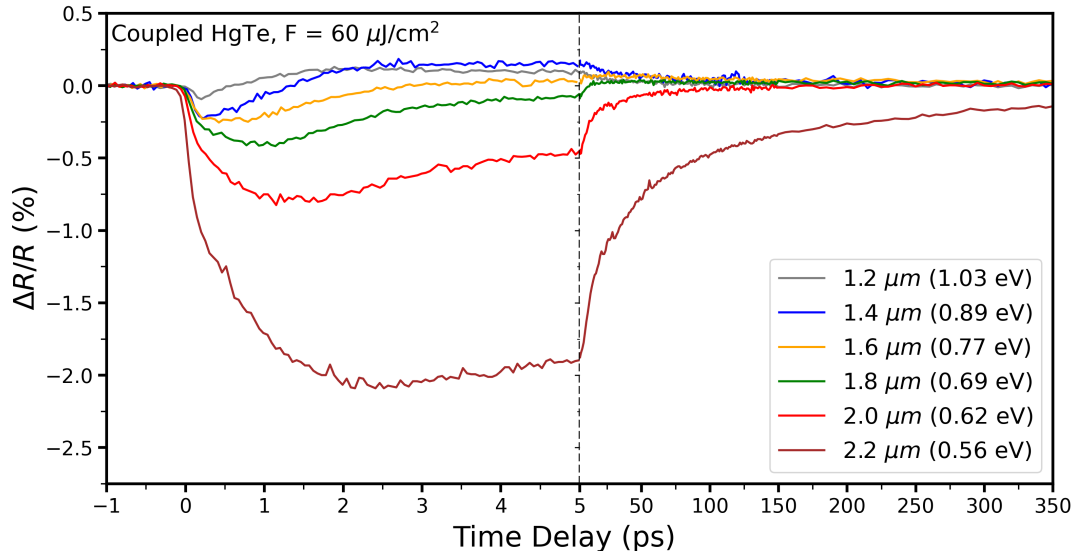


FIG. S7: Transient reflectivity versus pump-probe time delay without normalization for coupled HgTe QDs, at a pump fluence of $60 \mu\text{J}/\text{cm}^2$.

VIII. BIBLIOGRAPHY

-
- [1] N. Moghaddam, C. Gréboval, J. Qu, A. Chu, P. Rastogi, C. Livache, A. Khalili, X. Z. Xu, B. Baptiste, S. Klotz, G. Fishman, F. Capitani, S. Ithurria, S. Sauvage, and E. Lhuillier, “The Strong Confinement Regime in HgTe Two-Dimensional Nanoplatelets,” *The Journal of Physical Chemistry C*, vol. 124, pp. 23460–23468, Oct. 2020.
- [2] P. Harrison and A. Valavanis, *Quantum wells, wires and dots: theoretical and computational physics of semiconductor nanostructures*. Chichester, West Sussex, United Kingdom ; Hoboken, NJ, USA: Wiley, fourth edition ed., 2016.
- [3] C. Cohen-Tannoudji, B. Diu, and F. Laloë, *Mécanique quantique - Tome I*. Savoirs actuels, Les Ulis Paris: EDP sciences CNRS éditions, nouvelle éd ed., 2018.
- [4] G. Allan and C. Delerue, “Tight-binding calculations of the optical properties of HgTe nanocrystals,” *Physical Review B*, vol. 86, p. 165437, Oct. 2012.
- [5] B. Alén, J. Bosch, D. Granados, J. Martínez-Pastor, J. M. García, and L. González, “Oscillator strength reduction induced by external electric fields in self-assembled quantum dots and rings,” *Physical Review B*, vol. 75, p. 045319, Jan. 2007.
- [6] E. Lhuillier, S. Keuleyan, and P. Guyot-Sionnest, “Optical properties of HgTe colloidal quantum dots,” *Nanotechnology*, vol. 23, p. 175705, May 2012.
- [7] C. Cabrera, D. Contreras-Solorio, and L. Hernández, “Joint density of states in low dimensional semiconductors,” *Physica E: Low-dimensional Systems and Nanostructures*, vol. 76, pp. 103–108, Feb. 2016.
- [8] P. Rastogi, A. Chu, T. H. Dang, Y. Prado, C. Gréboval, J. Qu, C. Dabard, A. Khalili, E. Dandeu, B. Fix, X. Z. Xu, S. Ithurria, G. Vincent, B. Gallas, and E. Lhuillier, “Complex Optical Index of HgTe Nanocrystal Infrared Thin Films and Its Use for Short Wave Infrared Photodiode Design,” *Advanced Optical Materials*, vol. 9, p. 2002066, May 2021.
- [9] J. Qu, M. Weis, E. Izquierdo, S. G. Mizrahi, A. Chu, C. Dabard, C. Gréboval, E. Bossavit, Y. Prado, E. Péronne, S. Ithurria, G. Patriarche, M. G. Silly, G. Vincent, D. Boschetto, and E. Lhuillier, “Electroluminescence from nanocrystals above 2 μm ,” *Nature Photonics*, vol. 16, pp. 38–44, Jan. 2022.
- [10] A. Al-Otaify, S. V. Kershaw, S. Gupta, A. L. Rogach, G. Allan, C. Delerue, and D. J. Binks, “Multiple exciton generation and ultrafast exciton dynamics in HgTe colloidal quantum dots,” *Physical Chemistry Chemical Physics*, vol. 15, no. 39, p. 16864, 2013.
- [11] V. I. Klimov, J. A. McGuire, R. D. Schaller, and V. I. Rupasov, “Scaling of multiexciton lifetimes in semiconductor nanocrystals,” *Physical Review B*, vol. 77, p. 195324, May 2008.